Proceedings of ASME Turbo Expo 2011
GT2011
June 6-10, 2011, Vancouver, British Columbia, Canada

GT2011-45368

SIMULATIONS AND MEASUREMENTS OF THE FLOW AND NOISE IN HOT SUPERSONIC JETS

Philip J. Morris[†], Dennis K. McLaughlin, Yongle Du, Ching-Wen Kuo
Department of Aerospace Engineering
Penn State University
University Park, PA, USA
Email: pjm@psu.edu

ABSTRACT

This paper describes a combined computational and experimental study of the noise of exhaust jets with operating conditions typical of high performance military aircraft engines. The numerical simulations use a hybrid RANS/LES approach for the turbulence modeling. Structured multiblock grids with non-matching interfaces are used to enable details of the nozzle geometry to be included. Dual time-stepping is used to advance the solution in time and multigrid and implicit residual smoothing is used to accelerate the convergence of the sub-iterations. The acoustic field is determined by integration over an acoustic data surface based on solutions to the Ffowcs Williams – Hawkings equation. Both the near and far acoustic fields are determined. Baseline nozzles and nozzles with chevrons for noise reduction are simulated. To simulate the effect of the chevrons, without using a body-fitted grid, an immersed boundary method is used. The companion experiments, whose measurements are used to assess the quality of the numerical simulations, are performed in an anechoic jet facility. The facility includes a forward flight stream and uses helium-air mixtures to simulate the effects of jet heating. Flow and noise measurements are described for both baseline and chevron nozzles. Comparisons are made between the numerical predictions and the measurements.

INTRODUCTION

This paper describes a combined computational and experimental study of the jet noise radiated by high performance military aircraft engines. These engine exhausts are characterized by extremely high velocities and temperatures. In addition, the jets usually operate in an off-design condition. This results in a shock cell structure in the jet plume. The interaction of the turbulence in the jet shear layers with this shock cell structure results in broadband shock-associated noise. The noise levels generated by high performance military aircraft engines are sufficiently high to cause hearing damage to personnel working close to the aircraft, such as on an aircraft carrier deck, even when hearing protection is worn. In addition, the noise causes annoyance to communities in the vicinity of military bases. The accurate prediction of the noise is a key element in the development of noise reduction strategies. In addition, it is important to be able to predict the effect of noise reduction devices. This paper describes a numerical methodology to predict the noise from supersonic heated jets, with and without noise reduction devices. A companion experimental program is also described. The measurements are used to assess the quality of the numerical simulations.

The next section describes the simulation methodology and some preliminary calculations to evaluate the calculations. This is followed by a description of the experimental facility and measurement technique and both flow visualization and noise measurements. Comparisons are then made between predictions and measurements for both baseline and chevron nozzles.

NUMERICAL SIMULATIONS

Simulation methodology

In order to make the most effective use of limited computer resources, a hybrid method combining advanced CFD technology with an acoustic analogy is used for realistic jet noise simulations. The approach focuses on accurately

[†] Address all correspondence to this author

Copyright © 2011 by ASME

resolving the larger turbulent eddies but, of necessity, sacrifices the accuracy of the simulation of the very fine turbulent structures in return for lower computational resource requirements. This approach is justified based on the observation that the former are the dominant noise sources for high speed jets, and the latter are associated with noise 20dB or more below that associated with the large scale turbulent structures.

As a first step, the URANS (Unsteady Reynolds-Averaged Navier-Stokes) equations are solved in general curvilinear coordinates to simulate the development of the unsteady turbulent noise sources in the jet flow. Following the idea of model-free LES computations [1], a new variant of Detached Eddy Simulation, which deactivates the turbulent model in the DES region and lets the numerical dissipation provide the removal of unresolved turbulent scales, is used for turbulence modeling to avoid excessive dissipation in the mixing layers. A similar approach is used by Shur *et al.* [2,3]. A fourth-order Dispersion-Relation-Preserving (DRP) scheme [4] is used for spatial discretization. A dual-time stepping method is used to advance the development of the unsteady turbulent jet flow, and multigrid and implicit residual smoothing are used to accelerate the convergence of the sub-iterations.

Figure 1 shows the geometry of a military-style facetted nozzle with chevrons. The design Mach number is M_d =1.5. Supersonic hot jet noise simulations are performed for both the baseline nozzle (without chevrons attached) and the chevron nozzle, to evaluate the noise reduction effect at M_j=1.36, 1.47 and 1.56, and a total temperature ratio of 3.0. Here, M_j is the fully-expanded jet Mach number, The nozzle has an exit to throat area ratio of 1.18, and 12 chevrons are attached at the nozzle exit to match the facetted inner contours. The chevrons have a penetration of 9% of the nozzle exit diameter D, a length of 26% D, and a width of 80% percent of the facet width. In contrast with previous research by other authors [2, 3], realistic geometric details, including the facetted inner contours, the chevrons, and the finite nozzle thickness, are represented fully in the simulations.

A multiblock structured mesh with 5.88M grid points, as shown in Fig. 2, is created for the baseline nozzle simulations. A finite nozzle thickness is included. This is believed to help to trigger the unsteadiness in the initial jet shear layer. The grids are refined significantly around the jet potential core. The average grid sizes are 0.024 D from the nozzle exit to x/D = 4, and 0.047D from x/D=4 to x/D=10, which gives an estimate of the highest resolvable Strouhal number of approximately 4.0 if it is assumed that 7 points per wavelength are required to resolve the shortest wave components.

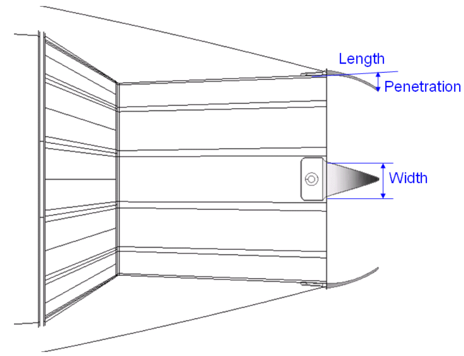

Figure 1. A military-style facetted nozzle with chevrons. (Only 4 out of 12 chevrons are shown for clarity)

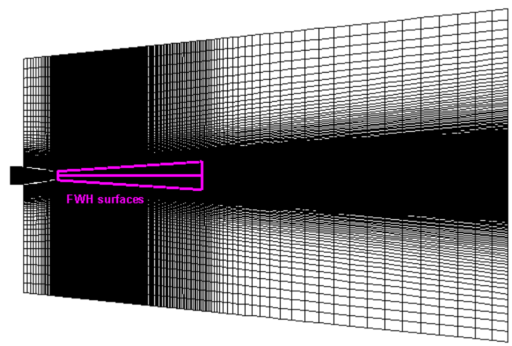

(a) Grids in the symmetry plan and the FWH surfaces

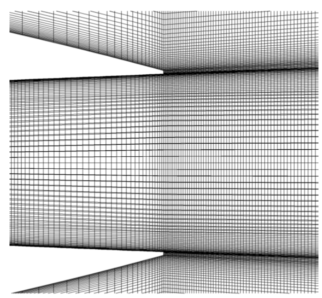

(b) Grid details at the nozzle exit in the symmetry plane

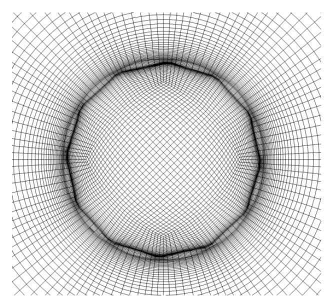

(c) Grid details near the nozzle exit in the axial station

Figure 2. Computational mesh and FWH surfaces

A difficulty with chevron nozzle simulations is the creation of a fully body-conformal mesh around the small chevron geometries. Therefore, the present approach uses the Immersed Boundary Method (IBM) [5] to represent the effects of chevrons on the unsteady jet flow and its noise radiation. In the IBM, some grid points are allowed to be immersed in the solid body, and the governing equations are modified on these immersed grid points to simulate the presence of solid bodies. Theoretically, the finer the grids are around the solid body, the more accurate the IBM will be. The Discrete-Time Derivation (DTD) of the Brinkman Penalization Method [6] is used for the immersed boundary condition implementation. The mass and energy equations are left unchanged, and the momentum

Copyright © 2011 by ASME

equations are modified at the grid points inside the solid body. Specifically, the momentum at the immersed grid points is set to zero and kept unchanged during the computation.

Figure 3 shows the grid details for the chevron nozzle simulations. To minimize grid effects on the evaluation of any noise changes, the same mesh for the baseline nozzle simulations is used. However, a small region around the chevrons is refined significantly to improve the accuracy of the IBM. Three times the number of grid points are used in the circumferential direction, and double the number of grid points are used in the radial direction, as compared with the grid density in the main computational domain. As a result, multiple non-matching block interfaces are created at the interfaces with the surrounding blocks, and a non-matching block interface condition must be used for flow variable communication. The IBM representation of the chevron geometries is shown in Fig. 4, where the grid points immersed inside the chevron geometries are shown with red colors.

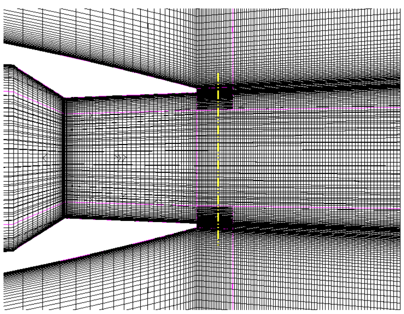

(a) Grid details at the nozzle exit in a symmetry plane

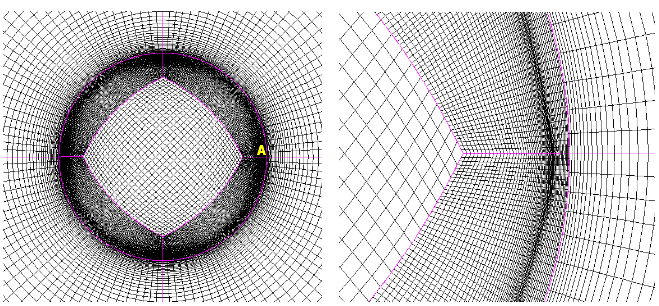

(b) Grid details near the nozzle exit at an axial station

(c) Grid details around the block intersection A

Figure 3. Computational mesh for chevron nozzle simulations

Since the spatial derivatives of the flow variables along some block interfaces are not continuous, special treatments are required. Kim and Lee [7] proposed a Characteristic Interface Condition (CIC) based on Thompson's Method of Characteristics boundary conditions [8]. At the block interface, a one-sided difference scheme is used to compute the spatial derivatives of the flow variables in the normal direction for each block. Then, the derivatives are corrected using the values from the block's neighbor if the characteristic waves are propagating into this block. The corrections are made such that the time derivatives of the flow variables are the same for each pair of matching grid points on the block interface.

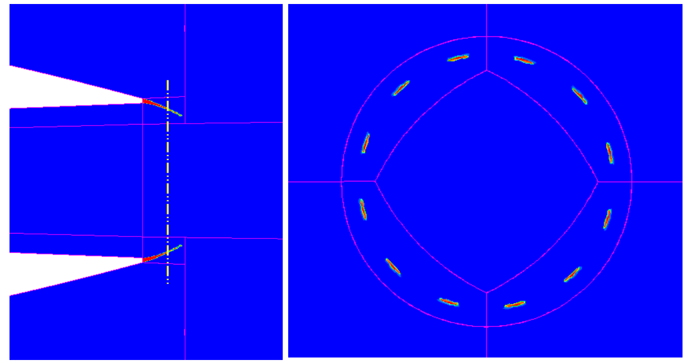

(a) A symmetric plane through one chevron tip

(b) An axial cross-section at 50% of the chevron length

Figure 4. The IBM representation of the chevron geometries. The region with red color shows the immersed grid points.

It should be noted that Kim & Lee's original equations are not easy to implement, especially when the mesh-orientations are not the same across the block interface. The present approach makes modifications to directly manipulate the residuals of the conservative form of the Navier-Stokes equations.

The corrected conservative form of the Navier-Stokes equations at the block interface can be written as:

$$\frac{\partial Q}{\partial t} + PS(L^* + Sc) = 0, \tag{1}$$

where, an asterisk is used to denote the value after correction. The corrected form of residuals is defined by:

$$\begin{aligned} \mathrm{Res}^* &= PS(L^* + Sc) - PS(L + Sc) + PS(L + Sc) \\ &= PS\Delta L + \mathrm{Res} \end{aligned} \tag{2}$$

where the corrections to L for the left block are,

$$\begin{aligned} \Delta L_i^l &= (L_i^r + Sc_i^r - Sc_i^l) - L_i^l \\ &= (S^{-1}P^{-1}\mathrm{Res})^r - (S^{-1}P^{-1}\mathrm{Res})^l \\ &= (S^{-1}P^{-1})^l(\mathrm{Res}^r - \mathrm{Res}^l). \end{aligned} \tag{3}$$

This formulation can be shown to be correct for arbitrary mesh orientations. For the non-matching block interfaces, the flow variables at the neighbor's grid points are first calculated by a high-resolution interpolation method, and then transferred to the neighbor block for boundary condition implementation.

Once the unsteady turbulent jet flow has reached a statistically stable state, the flow solutions are sampled every two physical

Copyright © 2011 by ASME

time steps on a set of integration surfaces surrounding the shear layers. Based on the permeable surface Ffowcs-Williams & Hawkings solution, the numerical integration of the unsteady flow solution at the retarded time gives the time-history of the acoustic pressure at a far-field observer [9,10].

SIMULATION RESULTS

This section describes the results of the studies using the methodology described in the previous section. Detailed comparisons with experiments for the radiated noise are given in a later section.

Effect of grid refinement

In preliminary research, a coarse mesh with 3.5M grid points was created. Compared with the fine mesh, the grid sizes in the streamwise and radial directions are reduced by half. Estimates of the highest resolvable Strouhal numbers are 2.0 for the coarse mesh, and 4.0 for the fine mesh, respectively.

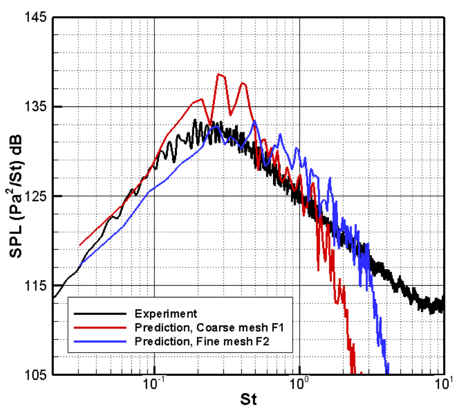

Figure 5. Comparison of the predicted noise spectra at the observer angle 60° and R/D=100 for the baseline nozzle jet operating at *Mj*=1.56, NPR=4.0, TTR=3.0.

Figure 5 shows a comparison of the predicted noise spectrum at an observer angle 60° and R/D=100 with experimental measurements from NASA Glenn Research Center [11,12]. A good agreement can be observed up to Strouhal number St≈1.5 for the coarse mesh, and St≈3.0 for the fine mesh. The increased resolution at higher frequencies is attributed to the smaller turbulent eddies resolvable by the fine mesh, as can be identified from the instantaneous vorticity contours shown in Fig. 6.

The time-mean flow solution is calculated by averaging the instantaneous flow over many physical time steps. The flow sampling is started at the same time as the sampling on the FWH surfaces for noise predictions. The variation of centerline axial velocity, and the turbulent kinetic energy (defined by $k = u'^2 + v'^2 + w'^2$) along the jet centerline and lip

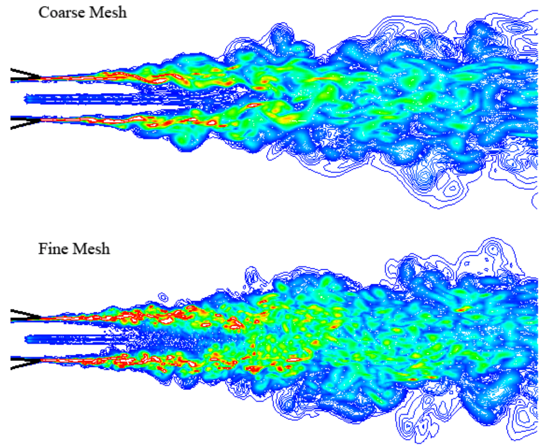

Figure 6. Comparison of instantaneous vorticity contours from the coarse and fine mesh computations for the baseline nozzle jet operating at *Mj*=1.56, NPR=4.0, TTR=3.0

lines are shown in Fig. 7. Because of the higher spatial resolution in the fine mesh, it allows the larger turbulent motions to break down into smaller eddies. Therefore it predicts less turbulence intensity along the centerline and the lip line, and thereafter a longer jet potential core.

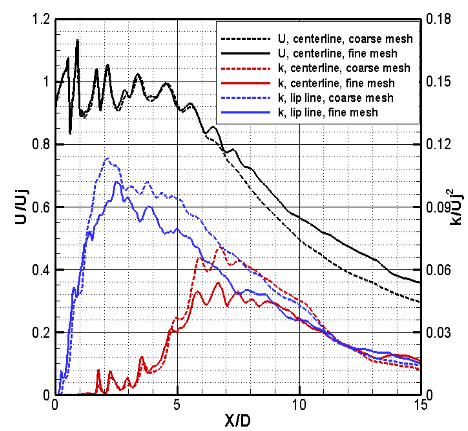

Figure 7. Comparison of time-averaged axial velocity and turbulent kinetic energy along the centerline and lip line from the coarse and fine mesh computations for the baseline nozzle jet operating at *Mj*=1.56, NPR=4.0, TTR=3.0

Effect of the location of the FWH surfaces

The usual implementation of the FWH theory essentially assumes that the noise sources outside the control surface can be neglected. In practice, terminating the streamwise extent of the control surface with a closing disk, which cuts the developing jet plume, and placing the control surface close to the shear layer always violates this assumption. Extending the

Copyright © 2011 by ASME

size of the acoustic data surfaces would be beneficial, but will inevitably increase the mesh size if a fine grid resolution is to be maintained. Therefore, most research compromises the resolution in return for an affordable computational load. The present research examines the impacts of the FWH surfaces with different radial and axial extents on far-field noise predictions. A similar study has been performed by Shur *et al.* [2], who proposed a new variant of the FWH equation to alleviate the influence of the location of the FWH surface on the noise prediction [13].

Several FWH surfaces with different axial and radial extents have been used in the present simulations, as shown in Fig. 8. Included are also the instantaneous vorticity contours, which indicate that the majority of the noise sources have been included in the closed FWH surfaces. The effects of different sizes of the FWH surfaces can be evaluated by examining the predicted noise spectra at different observer angles. In the first set, the three FWH surfaces, *L1W2*, *L2W2*, *L3W2* have the same radial extent, but are terminated at different downstream locations *X/D≈20*, *X/≈25* and *X/D≈30*, respectively. While in the second set, three surfaces *L2W1*, *L2W2*, *L2W3* are terminated at the same downstream location *X/D≈25*, but have

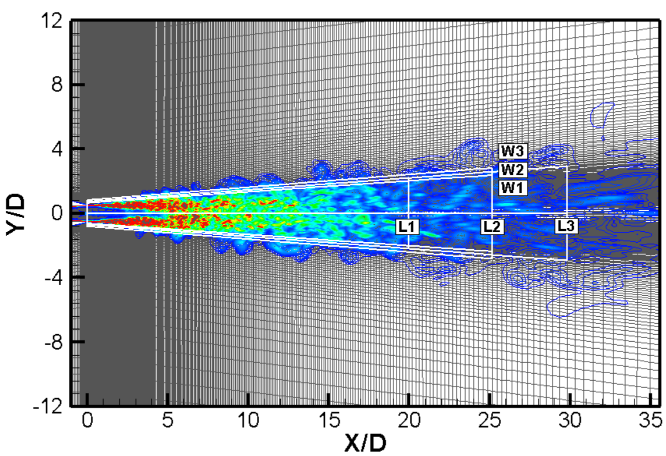

Figure 8. The FWH integration surfaces with different axial and radial extensions for the baseline nozzle jet operating at *Mj*=1.56, NPR=4.0 and TTR=3.0. The color contours show the instantaneous vorticity.

different radial extents. All surfaces have the upstream and downstream ends closed. As suggested by Spalart et al. [13], and demonstrated in a preliminary study, using an open surface would incur large low-frequency errors from the pseudo-sound generated by the convection of relatively slow vortices in the vicinity of the downstream end of the FWH surface.

Figure 9(a) shows the predicted noise spectra at four different observer angles using the FWH surfaces with different axial extents. Although the high-frequency noise spectra are almost identical, a large difference is observed at

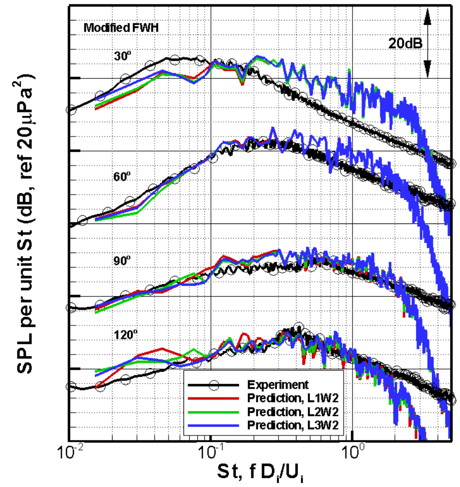

(a) Effects of the axial extent of the FWH surfaces

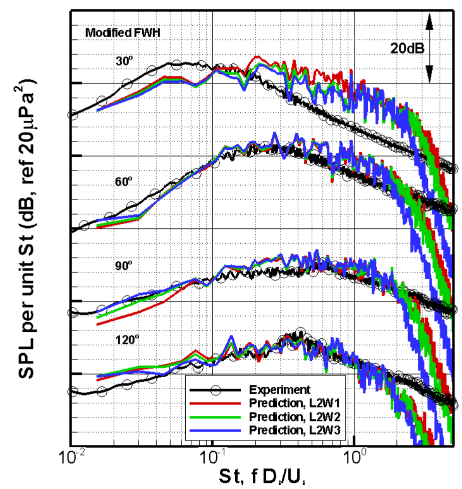

(b) Effects of the radial extent of the FWH surfaces

Figure 9. Comparison of predicted noise spectra using different axial and radial extents of the FWH surfaces for the baseline nozzle operating at *Mj*=1.56, NPR=4.0 and TTR=3. 3000 samples are used in each prediction.

low frequencies for all observer angles. Generally, the longer the FWH surface, the better the agreement with the experimental measurements. The impact of the different radial extents is shown in Fig. 9(b). A rapid drop of SPL at high frequencies is observed as the radius of the FWH surface increases. Considering that the grids are gradually stretching in the radial direction, the high-frequency acoustic energy is filtered by the excessive dissipation of the shorter sound waves while propagating to the control surfaces. A slight difference at low frequencies is attributed to the increased size of the downstream disk. These tests indicate that the length of the FWH surfaces is important for the low-frequency noise prediction, while the radial size of the FWH surfaces is critical for the high-frequency noise prediction. Considering these

Copyright © 2011 by ASME

effects, the integration surface *L3W2* is used in the remaining predictions in the present study.

Chevron nozzle simulation

The effect of chevrons on the jet flow can clearly be identified from the iso-surfaces of the streamwise vortices in Fig. 10, where the red iso-surface indicates a counter-clockwise rotating vortex and the blue color indicates a clockwise rotating vortex, when viewed from the downstream direction. Clearly, a pair of strong vortices is created behind each chevron. The vortex structures break down at the downstream position $x/D \approx 2.0$. Therefore, a significant change of the jet flow is observed within the first 2.0 diameters. It should be noted that there are no flow measurements available for comparison at this operating condition. To quantitatively compare the noise reduction effect of chevrons, a baseline nozzle computation at the same operating condition has been run.

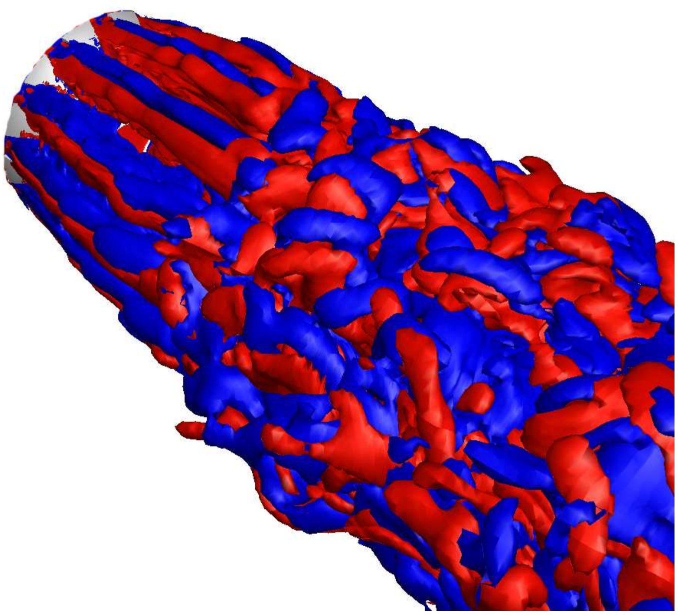

Figure 10. Three-dimensional view of the iso-surfaces of the streamwise vorticity for the chevron nozzle jet operating at Mj=1.47,NPR=3.5, TTR=3.0. Two values with the same magnitude are shown. Red: positive; blue: negative. The silver surfaces represent the chevron geometries.

For a clearer view of the noise generation mechanisms, Fig. 11 shows a snapshot of the density gradients and the pressure time-derivatives of the over-expanded M_j=1.47 jets issuing from the chevron nozzle, as well as the baseline nozzle. While the view of density gradients illustrates the shock cell structures in the jet plume, the pressure time-derivatives show the propagation of acoustic waves. An alternating compression-expansion flow pattern clearly presents in the

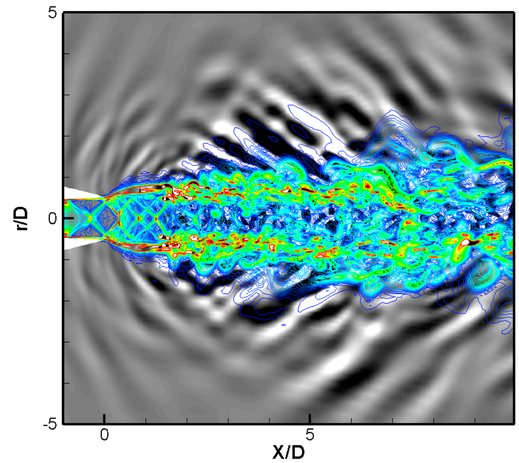

(a) Chevron nozzle, a chevron-valley plane

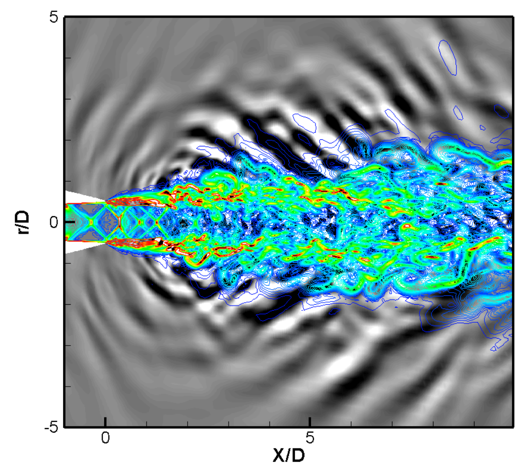

(b) Chevron nozzle, a chevron-tip plane

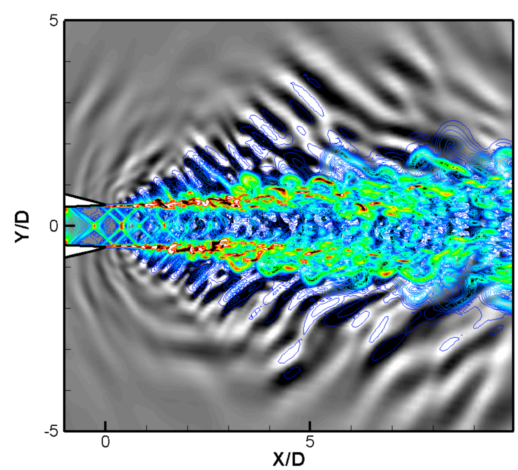

(c) Baseline nozzle, in a symmetry plane

Figure 11. Views of the instantaneous contours of density gradients (colored contours) and pressure time derivatives (grayscale backgrounds) of the over-expanded jet operating at Mj=1.47, NPR=3.5, TTR=3.0.

Copyright © 2011 by ASME

azimuthal direction following the chevron geometries, which demonstrates that the immersed boundary method correctly simulated the impact of chevrons on the jet flow. Although a similar double-shock structure is observed from both the chevron nozzle jet and the baseline nozzle jet, the presence of the chevrons significantly changes the shock cell structures in the first 2.0 diameters by destroying the second shock system originated from the nozzle throat and replacing it with another shock system originating from the chevrons. Compared with the baseline nozzle flow simulation, the chevrons are also found to enhance the turbulent flow mixing near the nozzle exit.

In Fig. 11, two distinct types of sound waves can be identified. The first is the strong Mach wave radiation seen propagating in the downstream direction, and the other is the lower level sound propagation in the upstream direction. Both are found to originate from near the nozzle exit. However, compared with the baseline nozzle jet, the strong Mach wave radiation is weakened in the chevron jet due to the enhanced turbulent mixing near the nozzle exit.

EXPERIMENTS

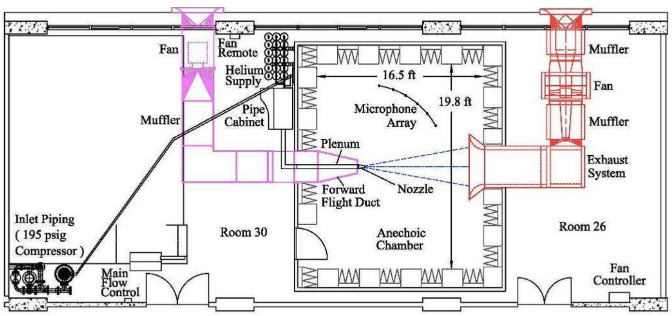

Figure 12(a). Schematic of The Pennsylvania State University high speed jet noise facility.

The Pennsylvania State University high speed jet noise facility was used for the experiments presented in the current study. The facility schematic is shown in Fig. 12(a). High pressure air, pressurized by a *CS-121* compressor combined with a *KAD-370* air dryer both manufactured by *Kaeser Compressors*, is provided from the tank, and then the air flow is regulated via pressure regulators and control valves located in a piping cabinet. A helium supply is connected to the piping cabinet where helium is mixed with air in order to simulate heated jets. The individual partial pressures of the helium and air are both regulated in the piping cabinet to predetermined values to accurately match the acoustic velocity of the hot jet condition being simulated. Following the piping cabinet the He-air mixture is fed to the jet plenum and exhausted through a nozzle into the anechoic chamber. A pitot probe is embedded in the middle section of the plenum to provide, with a pressure transducer, the total pressure upstream of the nozzle. The operating procedure for the He-air mixtures was developed by Doty and McLaughlin [14].

The anechoic chamber walls are covered with fiberglass wedges and have an approximate cut-off frequency of 250 Hz. An exhaust collector and fan on the opposite wall of the plenum in the anechoic chamber prevents flow recirculation and possible helium accumulation. Acoustic measurements are currently performed using six microphones, hanging from a boom that extends from the plenum stand, as can be seen in the image of Fig. 12(b). The microphone array rotates freely around a point located at the center of the nozzle exit plane. The microphones are positioned at a grazing incidence to the jet centerline and equally spaced by 10 degrees. The average physical radial distance of microphones to the nozzle exit is approximately 1.78 m (70 in). This distance is sufficient for the microphones to be considered in the far field [15,16] when testing nozzles less than 2.5 cm (1 in) in diameter operate in this facility. The microphones are 1/8” pressure-field microphones selected to match the nozzles sizes used in this small scale facility: type 4138 from *Brüel and Kjaer* (*B&K*), and type 40DP from *GRAS*. Following calibration corrections,

Figure 12(b). Photograph of The Pennsylvania State University high speed jet noise facility.

the acoustic data have a frequency response reliably accurate to 120 kHz. This is adequate to define the acoustic frequencies most important to noise studies, including those approximately a factor of 10 higher than the peak frequencies in the maximum noise emission direction. The range is not adequate to fully define the noise spectra to the highest non-dimensional frequencies that are typically much less important in supersonic aircraft noise. The acoustic measurements are performed from polar angle θ = 30° to θ = 120° measured from the jet downstream direction originating at the nozzle exit plane, with increments of 10 degrees.

Data processing and comparison procedure

A flow chart of the data acquisition process is shown in Fig. 13. The microphone calibration is performed with a *B&K*

Copyright © 2011 by ASME

acoustic calibrator, model 4231, and the microphone calibration constants are recorded to provide the conversion from the measured voltages to the equivalent pressure. The

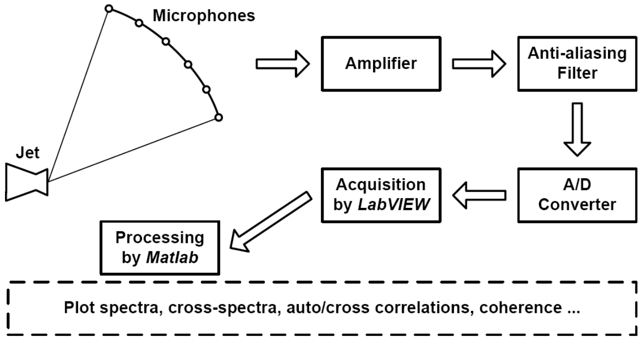

Figure 13. Flow chart of the data acquisition process.

analog time-domain signals from the microphones are routed through a *Nexus*, *B&K* signal conditioner or a *GRAS* model 12AN power module and then amplified and filtered for anti-aliasing, thus enabling their accurate digital conversion in the following acquisition. A high-pass filter is also set to 500 Hz, removing any undesirable low frequency noise that could contaminate the data. A PCI-6123 *National Instruments* DAQ board acquires the time domain data which are then stored in binary files. The sampling rate is set at 300 kHz and 102,400 to 409,600 data point are collected, the reduced dataset being used for helium-air mixture jets in order to reduce the amount of helium used during an experiment. The raw data are then fed into *Matlab* for data processing. The raw data are split into 1024 or 4096 points segments and a Hanning window is applied with 50 percent overlap between each window. The Fast Fourier Transform is calculated in each window and an averaged value is calculated from the 199 segments. This yields the power spectral density (*PSD*) which is then converted to a decibel (dB) scale using a reference pressure of 20 μPa. Three corrections are then applied to the raw sound pressure level (*SPL*) to compute the lossless *SPL* as explained in Kuo *et al.* [17]. Finally, the spectra are non-dimensionalized to *SPL* per Strouhal number. Equation (4) summarizes the different steps that lead to the *SPL* per unit Strouhal number.

$$SPL(St) = SPL_{raw}(Hz) - \underbrace{\Delta C_{act}(Hz) - \Delta C_{ff}(Hz)}_{\text{Microphone Corrections}} + \underbrace{\Delta C_{atm}(Hz)}_{\text{Atmospheric Correction}} + \underbrace{10 \times \log_{10} f_C}_{\text{Strouhal Number Scaling}}. \quad (4)$$

The experimental data are processed into lossless spectra per unit Strouhal number to enable comparisons easier across scales. The majority of the measurements are made at distances of approximately R_{raw} = 100 D depending on the nozzle diameter. Following processing, the resulting data are (back) propagated to R = 100 D assuming spherical spreading of the acoustic field to allow direct comparison of data at a common observer distance. This “back” propagated *SPL* is determined from

$$SPL(St) = SPL(St)_{raw} + 20log_{10}(R_{raw} / R) \quad (5)$$

The Strouhal number is defined as $St = f / f_c$, with f_c the characteristic frequency of the jet defined by $f_c = U_j / D_j$, where U_j is the mean jet velocity, and D_j is the fully expanded diameter of the jet plume.

Heated jet simulation

The density characteristics of heated jets are replicated using gas mixtures in order to produce acoustic measurements in cold small scale facilities that can be compared directly to hot moderate scale experiments or actual aircraft engine measurements. Kinzie and McLaughlin [18] demonstrated that the mixture of helium and air is able to capture the dominant noise characteristics of actual heated jets. Doty and McLaughlin [14] and Papamoschou [19] have shown that mixtures of helium and air can appropriately simulate the noise of heated jets to an excellent accuracy by matching the acoustic velocity of the heated gas. Recently, Miller and Veltin [20] showed a good agreement of the flow properties between the experimental data from helium-air mixture jets and numerical simulations of heated air jets. The features of heated jets are lowered density and increased acoustic velocity (for a given nozzle pressure ratio), and both of these features are reproduced by helium-air mixture jets.

Geometry of military style supersonic nozzles

The experimental results have been obtained with the military style nozzles representative of the exhaust of aircraft engines of the F404 family. The inner contours of the military style nozzles have been provided by General Electric Aviation. These nozzles are the geometries as used in the numerical simulations. At Penn State, the nozzles have been fabricated using rapid prototyping techniques. These military style supersonic nozzles were built with the identical inner geometry at small and moderate scale to demonstrate the scaling of small heat simulated jets to moderate and full size jets. More details of these military style supersonic nozzles can be found in Kuo *et al*. [21]. In general, the expansion portion of the flow contour consists of 12 flat segments that are interleaved to facilitate area adjustment of the operational nozzles. Unlike well designed contoured CD nozzles, the more realistic nozzles result in a plume with weak shock cells, even at perfectly balanced pressure conditions based on area ratio.

The chevron configurations were designed and provided by General Electric Aviation and NASA Glenn Research Center. The chevrons extend from the nozzle exit plane of the baseline nozzles with one chevron per facet (totaling 12).

Copyright © 2011 by ASME

Experimental results for the Military-style CD chevron nozzle

Measureable noise reduction was achieved with the M_d =1.5 GE nozzle with the chevrons operating at the under-expanded jet Mach number of M_j =1.64. Figure 14 shows the spectral comparison and *OASPL* contour at a range of polar angles between the small scale chevron nozzle jet and the baseline identical nozzle jet (without chevrons) both operating with pure air cold M_j =1.64 jet. A substantial level of noise reduction was observed. Most of the noise reduction is experienced in the downstream arc, in the maximum noise emission direction, where the generated sound is contributed by the large scale turbulence noise. There is a shift in the peak BBSAN frequency to higher frequencies with the chevron configuration, as well as a decrease in amplitude. This suggests smaller shock cells and weaker shocks, and results in a noise reduction on the sideline. Overall, the *OASPL* noise reduction varies from 2 to 4 dB across the polar angle range measured. At this point it appears that the small scale chevron nozzle experiments produce noise reductions that are comparable to those measured by Henderson and Bridges [11] at NASA. Figure 15 shows the schlieren images of both baseline and chevron nozzles operating with pure air cold: M_j =1.64 jet. The amplified jet spreading (due to the chevrons) leads to increased jet mixing in the initial jet shear layer. This contributes to the redistribution of jet momentum in the initial shear layer. The corresponding results (as shown in Fig. 14) are the noise reduction attributed to the suppression of the Mach wave radiation in the jet downstream direction.

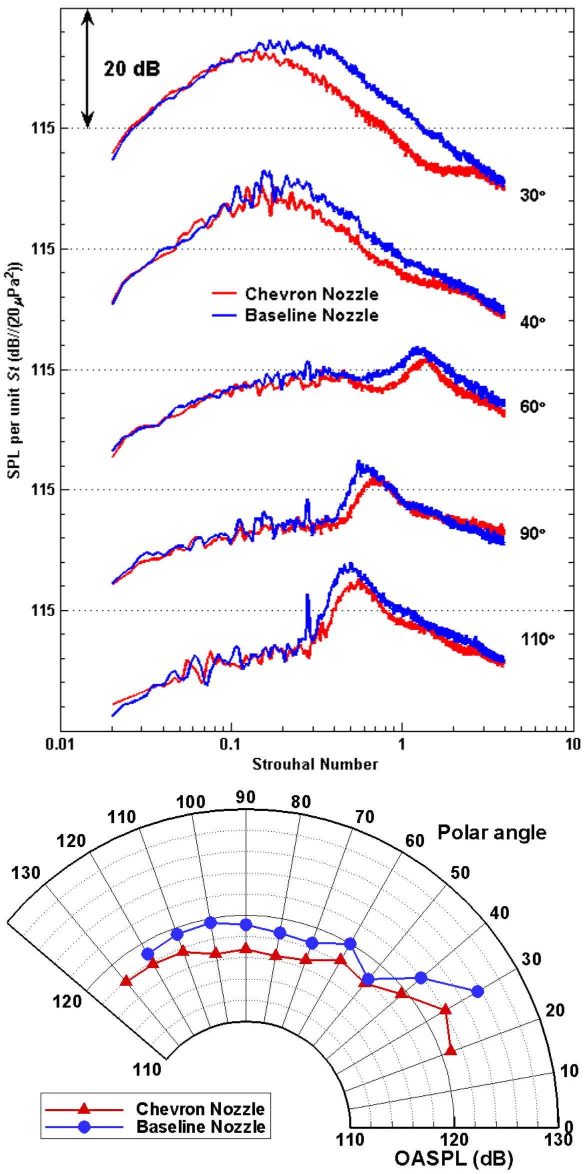

Figure 14. Acoustic spectra and *OASPL* from the measurements conducted with GE M_d =1.5 baseline and chevron nozzles operated under-expanded at M_j = 1.64, *TTR* = 1.

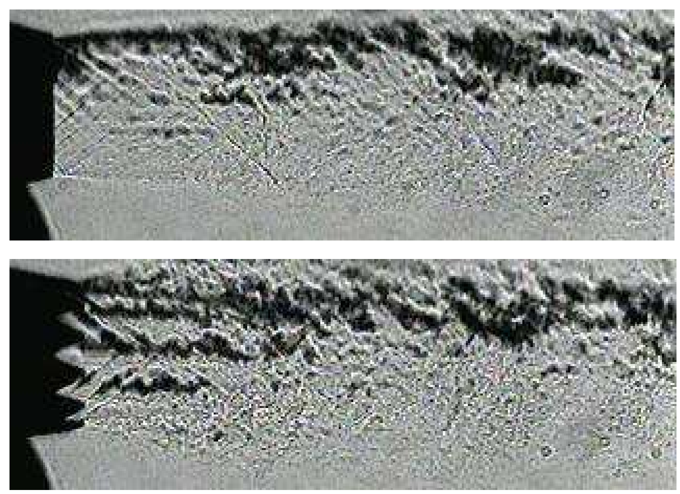

Figure 15. Schlieren images conducted with GE M_d =1.5 nozzles (baseline - top, chevron - bottom) operated at M_j =1.64, *TTR* = 1.

Figure 16 shows a similar spectral comparison and *OASPL* contour of data recorded at the same conditions as the data of Fig. 14 except the jet is operated with a total temperature ratio of *TTR* = 3.0, where a helium-air mixture has been used at Penn State. Under this condition, the noise reduction is noticeably less, with maximum levels of approximately 1.5 dB in the maximum noise emission direction. No perceivable benefit is observed in the sideline direction. Since heat (and helium) affects the jet mixing layer by making it thicker, it is understandable that the increased mixing provided by the chevrons has less effect. Similarly, the BBSAN component is much less dominant in a heated jet on the sideline, due to 1) the increased level of the turbulence mixing noise (caused by a higher jet acoustic Mach number), and 2) the increased mixing layer thickness that weakens the shock cell strength. Therefore, the previously observed shift of the BBSAN frequency and decrease in amplitude is much less

Copyright © 2011 by ASME

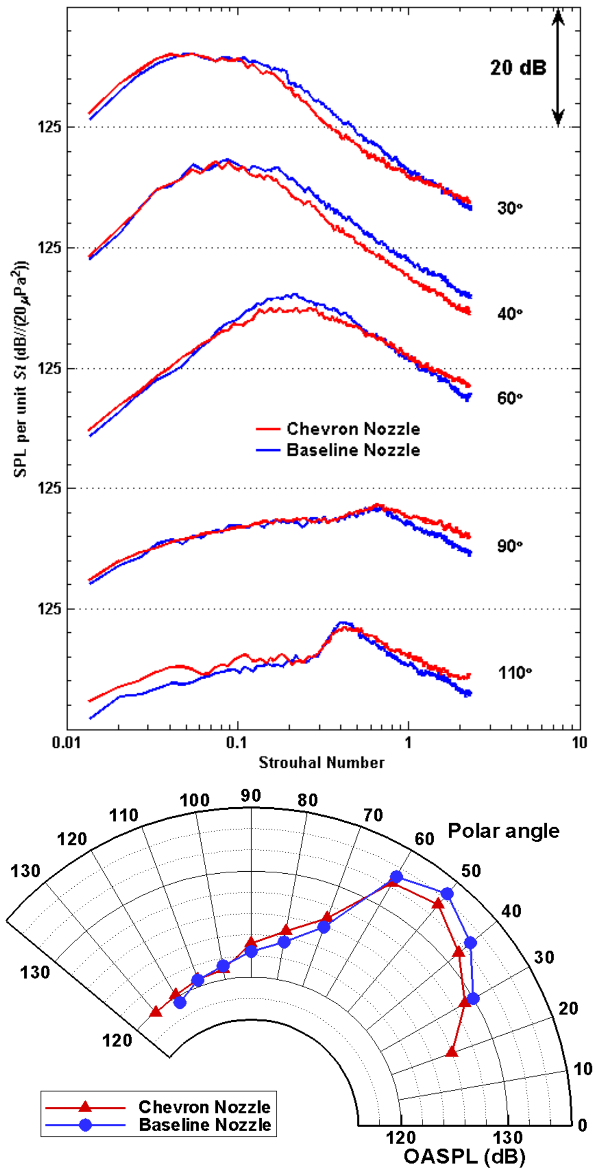

Figure 16. Acoustic spectra and *OASPL* from the measurements conducted with GE M_d =1.5 baseline and chevron nozzles operated under-expanded at M_j =1.64, *TTR* = 3.

apparent and has no effect on the *OASPL* in the sideline and jet upstream directions. An extended study focuses on effects of supersonic jet conditions on broadband shock-associated noise can be found in Ref. [22].

Figure 17 shows the schlieren images of both baseline and chevron nozzles operating with pure air cold M_j =1.47 jet. The jet spreading in the chevron nozzle jets displays slight amplification in the initial jet shear layer. It was found that there is a modest noise reduction from the measurements of the

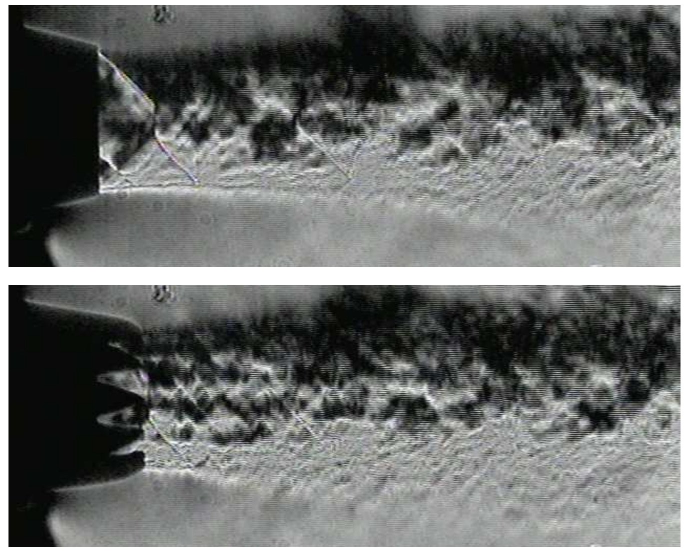

Figure 17. Schlieren images obtained with GE M_d =1.65 nozzles (baseline - top, chevron - bottom) operated at M_j =1.47, *TTR* = 1.

chevron nozzle operating in the small-scale over-expanded jet. Additional Penn State experimental data on the effects of chevrons on the supersonic jet noise are presented in Fig. 18. These data are presented for an over-expanded jet case, believed to be the more important condition for fighter aircraft take-off. Measureable noise reduction was achieved with the M_d =1.65 GE nozzle with the chevrons operating at the over-expanded jet Mach number of M_j =1.47, but the reduction is noticeably less that is found in moderate size jet experiments conducted at NASA Glenn Research Center [11]. The hypothesis for the less effective acoustics benefit (compared to moderate-scale jets) is the low Reynolds number of the small-scale jets. The lower Reynolds number leads to the earlier flow separation inside the nozzle divergent section. The location of the flow separation inside the nozzle wall therefore affects the efficiency of the chevrons. In an effort to clarify this hypothesis, the experiments that produced the data of Fig. 18 were conducted with nozzles with some internal roughness included to obtain some degree of turbulent boundary layer flow in the nozzle. More detailed experimental results and discussion on this issue are documented in Kuo *et al*. [21].

COMPARISONS OF SIMULATIONS AND EXPERIMENTS

For the majority of the jet simulations at different operating conditions performed in the present research, there are only far-field noise measurements available for comparison. The data presented are from measurements performed at both PSU and NASA GRC [11], with small-scale and moderate-scale

Copyright © 2011 by ASME

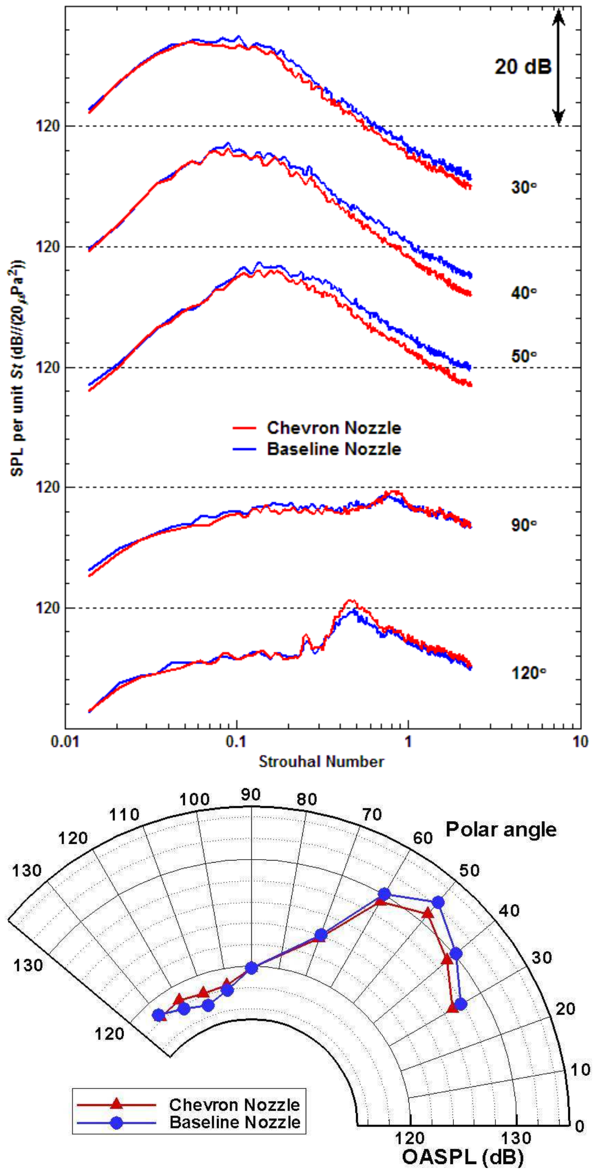

Figure 18. Spectral comparisons from the measurements conducted with GE M_d =1.65 baseline and chevron nozzles operated over-expanded at M_j =1.47, TTR = 3.0.

nozzles. Using the FWH theory, the far-field noise predictions are made based on the instantaneous near-field flow solutions of approximately 5800 samples. The predictions are compared with the measurements at PSU and NASA GRC as noted earlier. Considering that a 2~3dB deviation is usually observed for the noise spectrum and OASPL measurements of the same nozzle using different facilities or the different scale of nozzles using the same facilities [23,24], the agreement is believed to be "very good" if the disparity between the predictions and the experiments are within 3dB.

The noise spectra at different observer angles for the three jets are shown in Figs. 19-21. Each noise spectrum is shifted by 20dB relative to its neighbor observers for clarity. The small scale measurements conducted at Penn State were only available (in reliable form) for the first jet condition. The results do show good consistency with the NASA data providing additional confirmation of the ability of the small scale experiments to do a reasonable job of replicating the higher Reynolds number data. It was noted in an earlier paper [24] that the higher levels of noise in the low frequency end of the spectra is believed to be a result of the lower Reynolds number operating condition.

Focusing attention of the computational results, the agreement is very encouraging. The good agreement reaches St≈3 as expected since the computational grids are designed to resolve the highest frequency up to St≈4. The peak-noise frequency shift to the low-frequency range of the noise spectra as the observer angles increase is well captured for all three jets. Specifically,

- At all upstream directions θ>90º, the predictions have an good agreement with the experiment measurements. The frequencies and amplitudes of the BBSAN component are captured precisely. The discrepancies at discrete frequencies are less than 4dB.

- At all downstream directions θ≤90º, good agreement is found from St≈0.01 to St≈0.3 for all three jets. The maximum deviation from the measurements is within 4dB at several frequencies, while most are within 2dB. Computations show that the agreement at low frequencies is usually improved as more samples are accumulated for noise predictions.

- However, above the frequency of St≈0.3, an intriguing but consistent trend is observed. In the peak noise radiation directions, less than θ≈50º, the agreement becomes worse as the observer moves closer to the jet axis. The over-prediction increases from less than 2dB for the M_j=1.36 jet to more than 8dB for the M_j=1.56 jet. While, above the polar angle of the peak noise radiation direction, the agreement becomes better as the observer moves toward the sideline and into the forward arc. The over-prediction decreases from more than 8dB for the M_j=1.36 jet to less than 3dB for the M_j=1.56 jet.

- For all three jets, the agreements of the noise spectra at the peak noise radiation direction are as good as those at the upstream observers.

During the research, as mentioned earlier, many attempts were made to address the mismatch at frequencies above St≈0.3 by manipulating the grid distribution in the jet potential core, the artificial dissipation terms and the FWH surfaces.

Copyright © 2011 by ASME

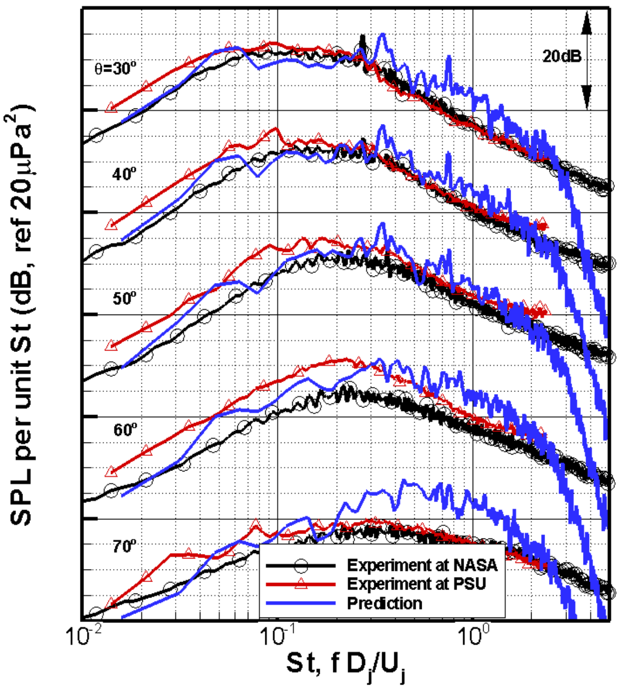

(a) 30º~70º

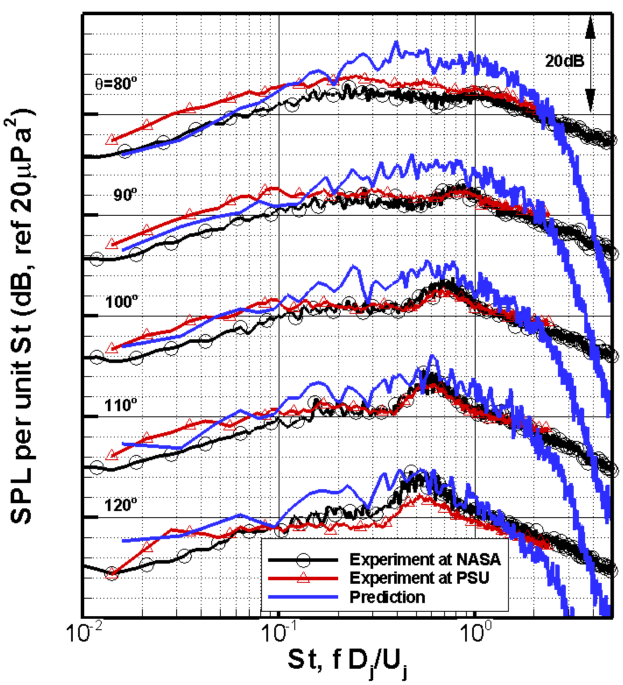

(a) 80º~120º

Figure 19. Comparison of the predicted noise spectra with the experiments at NASA GRC and PSU. Operating conditions: Mj=1.36, NPR=3.0, TTR=3.0

Unfortunately, the same consistent trend was observed. This mismatch requires additional research. However, a clue is

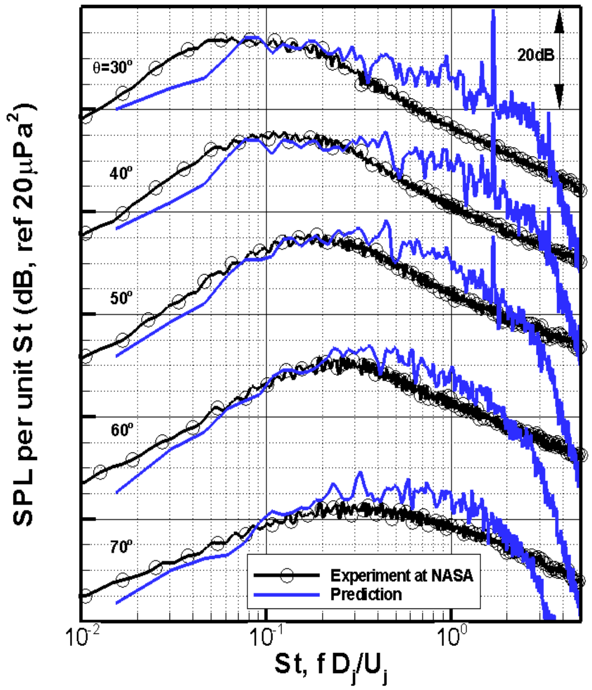

(a) 30º-70º, R/D=100

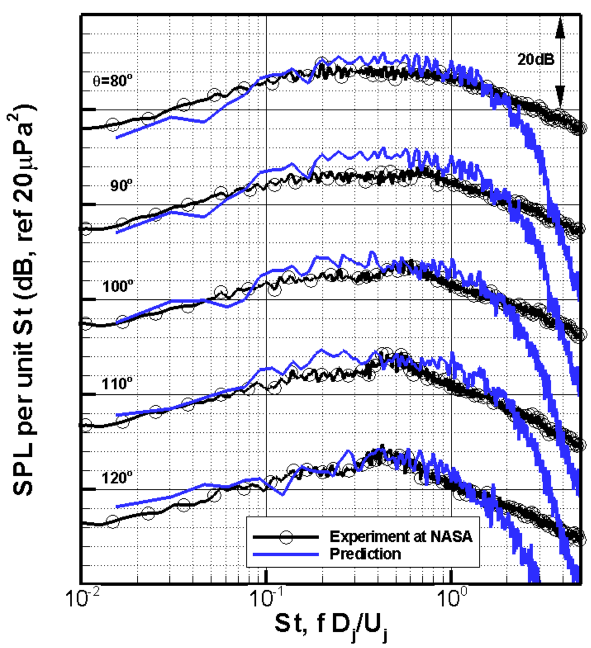

(a) 80º-120º, R/D=100

Figure 20. Comparison of the predicted noise spectra with the experiments at NASA GRC. Operating conditions: Mj=1.47, NPR=3.5, TTR=3

offered by the chevron nozzle calculations, which are presented next.

Copyright © 2011 by ASME

In Fig. 22, comparisons of the noise spectra are shown for the baseline nozzle jet and the chevron nozzle jet operating with Mj=1.47 and TTR=3.0. Although the measurements are not available at present, an experiment at a similar condition (M_d=1.65, M_j=1.47, TTR=3.0) [25] exhibits the similar high-frequency noise reduction at shallow observer angles, and slight noise reduction at sideline and upstream observer angles, except the fact that the experimental measurements did not show as much noise reduction at high-frequencies as shown in the noise prediction. At observer lower angles, the noise

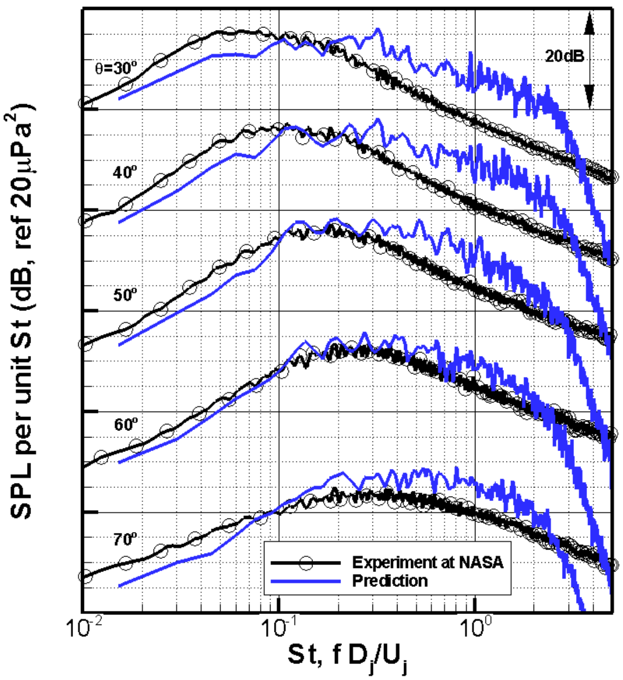

(a) 30º-70º, R/D=100

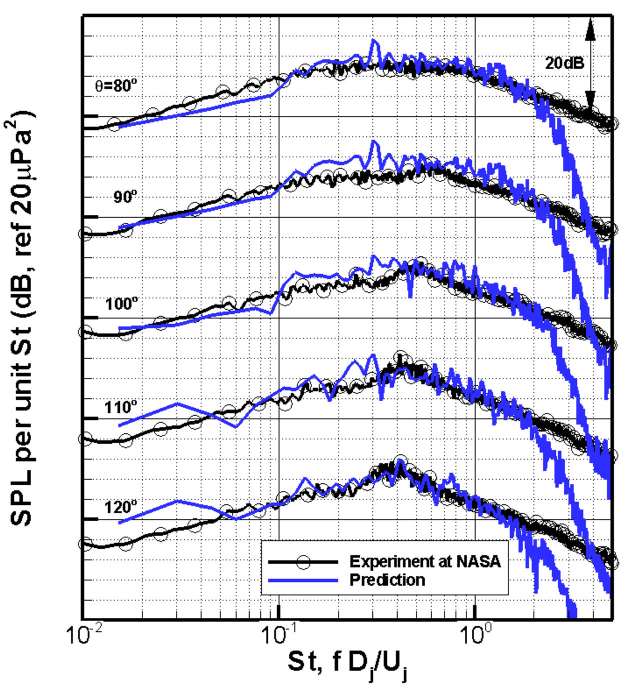

(b) 80º-120º, R/D=100

Figure 21. Comparison of the predicted noise spectra with the experiments at NASA GRC. Operating conditions: Mj=1.56, NPR=4.0, TTR=3.0

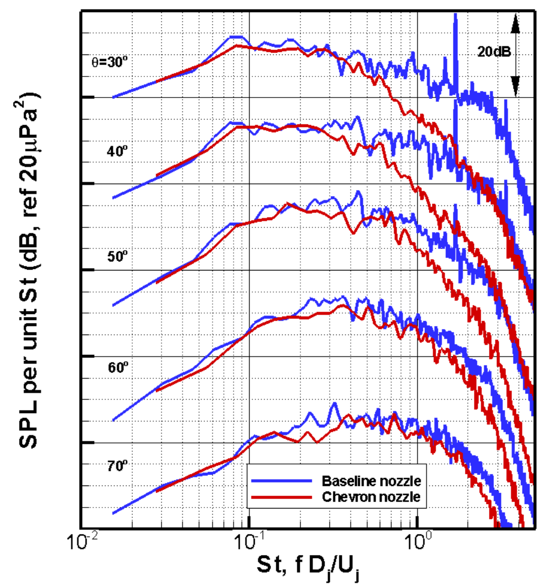

(a) 30º-70º, R/D=100

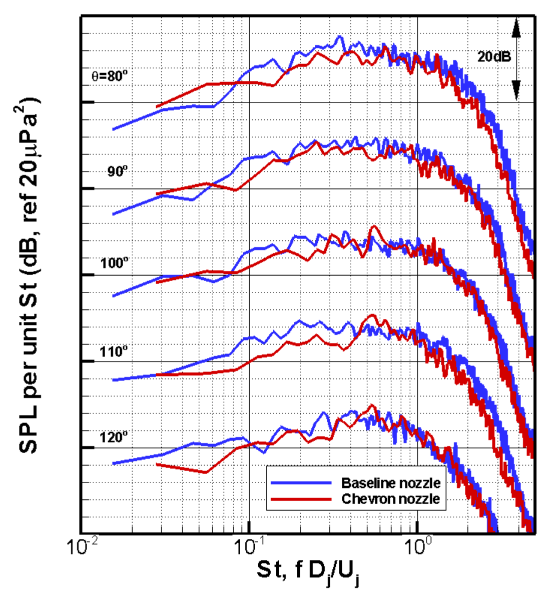

(b) 80º-120º, R/D=100

Figure 22. Comparison of the noise spectra of the baseline nozzle jet and the chevron nozzle jet operating at Mj=1.47, NPR=3.5 and TTR=3.0

Copyright © 2011 by ASME

spectra of the chevron nozzle jet appeared to agree better with the baseline nozzle measurements. Considering the facts that the computational grids and numerical methods are the same for the main flow field and that the only difference comes from the significantly refined grids around the chevrons, it is speculated that the azimuthal resolution of the baseline nozzle simulation can result in a different initial development of the turbulent shear layer, which might lead to an over-prediction of the noise spectra. The comparison of OASPL in Fig. 23 shows that nearly 4dB noise reduction is achieved at the peak noise radiation direction around θ≈50°. However, since the OASPL is over-predicted, as shown above, the actual noise reduction is likely to be less.

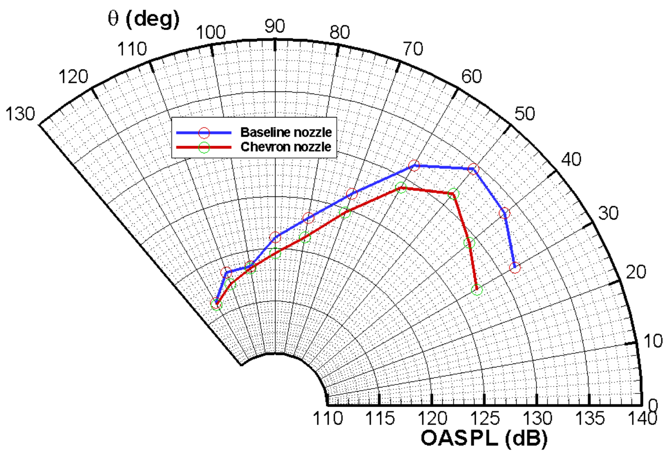

Figure 23. Comparison of the OASPL directivity of the baseline nozzle jet and the chevron nozzle jet operating at Mj=1.47, NPR=3.5, TTR=3.0

CONCLUSIONS

In the current research, a hybrid method is used for the noise simulation of supersonic hot jets of realistic military-style nozzles. Good agreement of the noise spectra with the experimental measurements is observed at most observer angles. With a moderate mesh size of 6M grid points, the highest resolved frequencies reach St≈3. More encouraging is that the frequencies and SPL of the broad-band shock-associated noise are precisely captured for all three jets. The immersed boundary method is used for chevron nozzle simulations without actually creating a body-conformal mesh for the chevrons, which significantly increases computation times. The simulation results captured the turbulent enhancing mechanism due to the presence of the chevrons. The noise reduction effect is also quite well predicted.

Though the present results are very encouraging, it is clear that further improvements in the accuracy of the simulations are required. Some of this is simply associated with increased overall grid resolution, as this will increase the range of Strouhal numbers that can be captured. The results of the chevron simulations also indicate the azimuthal resolution in the vicinity of the nozzle exit is a crucial parameter. The location and closure of the FWH acoustic data surface, though much recent research has provided useful information, should not be considered a closed question. Different implementations continue to suggest different trends and further investigation of this important problem is required.

ACKNOWLEDGMENTS

This research was supported originally by the Strategic Environmental Research and Development Program (SERDP). The program manager is Mr. Bruce Sartwell. Additional funding has been provided under an STTR with Innovative Technology Applications Company (ITAC), LLC, with support from the US Navy. The technical monitor is Dr. John Spyropoulos.

REFERENCES

[1] F. Grinstein, 2006. Recent progress on monotone integrated large eddy simulation of free jets. *JSME International Journal*, **49**(4), pp. 890-898.
[2] M. L. Shur, P. R. Spalart and M. K. Strelets, 2005. Noise prediction for increasingly complex jets. Part I: methods and tests. Part II: applications. *International Journal of Aeroacoustics*, **8**(3&4), pp. 213-266.
[3] M. L. Shur, P. R. Spalart, M. K. Strelets and A. V. Garbaruk, 2006. Further step in LES-based noise prediction for complex jets. AIAA Paper 2006-485.
[4] C. K. W. Tam and J. C. Webb, 1993. Dispersion-relation-preserving finite difference schemes for computational aeroacoustics. *Journal of Computational Physics*, **107**(1), pp. 262-281.
[5] R. Mittal and G. Iaccarino, 2005. Immersed boundary methods. *Annual Review of Fluid Mechanics*, **37**, pp. 239-261.
[6] J. Mohd-Yusof, 2007. Combined immersed-boundary/B-spline methods for simulations of flow in complex geometries. NASA/TM-2007-214853.
[7] J. W. Kim and D. J. Lee, 2003. Characteristic interface conditions for multiblock high-order computations on singular structured grid. *AIAA Journal*, **41**(12), pp. 104-129.
[8] K. W. Thompson, 1990. Time-dependent boundary conditions for hyperbolic systems, II. *Journal of Computational Physics*, **89**, pp. 439-461.
[9] J. E. Ffowcs Williams and D. L. Hawkings, 1969. Sound generated by turbulence and surfaces in arbitrary motion.

Copyright © 2011 by ASME

Philosophical Transactions of the Royal Society of London (A), **264**(1151), pp. 321-342.
[10] K. S. Brentner and F. Farassat, 1998. Analytical comparison of the acoustic analogy and Kirchhoff formulation for moving surfaces. *AIAA Journal*, **36**(8), pp. 477-491.
[11] B. Henderson and J. E. Bridges, 2010. An MDOE investigation of chevrons for supersonic jet noise reduction. AIAA Paper 2010-3926.
[12] J. E. Bridges, 2010. Personal communication.
[13] P. R. Spalart and Shur, M. L., 2009. Variants of the Ffowcs Williams - Hawkings equation and their coupleing with simulations of hot jets. *International Journal of Aeroacoustics*, **8**(5), pp. 477-491.
[14] M. J. Doty and D. K. McLaughlin, 2003. Acoustic and mean flow measurements of high-speed, helium-air mixture jets. *International Journal of Aeroacoustics*, **2**(2), pp. 293–334.
[15] L. D. Koch, J. Bridges, C. Brown and A. Khavaran, 2005. Experimental and analytical determination of the geometric far field for round jets. *Noise Control Engineering Journal*, **53**(1), pp. 20–28.
[16] K. Viswanathan, 2006. Instrumentation considerations for accurate jet noise measurements. *AIAA Journal*, **44**(6), pp. 1137-1149.
[17] C.-W. Kuo, J. Veltin and D. K. McLaughlin, 2009. Methods to improve the accuracy of acoustic measurements in small scale high speed jets. AIAA Paper 2009-3251.
[18] K. W. Kinzie and D. K. McLaughlin, 1999. Measurements of supersonic helium/air mixture jets. *AIAA Journal*, **37**(11), pp. 1363-1369.
[19] D. Papamoschou, 2007. Acoustic simulation of coaxial hot air jets using cold helium–air mixture jets. *Journal of Propulsion and Power*, **23**(2), pp. 375–381.
[20] S. Miller and J. Veltin, 2011. Experimental and numerical investigation of flow properties of supersonic helium-air jets. *AIAA Journal*, **49**(1), pp. 235-246.
[21] C.-W. Kuo, J. Veltin and D. K. McLaughlin, 2010. Advanced acoustic assessment of small-scale military-style nozzle with chevrons. AIAA Paper 2010-3923.
[22] C.-W. Kuo, D. K. McLaughlin and P. J. Morris, 2011. Effects of supersonic jet conditions on broadband shock-associated noise. AIAA Paper 2011-1032.
[23] J. Veltin, 2008. On the characterization of noise sources in supersonic shock-containing jets. PhD thesis, the Pennsylvania State University.
[24] D. K. McLaughlin, J. E. Bridges and C.-W. Kuo, 2010. On the scaling of small, heat simulated jet noise measurements to moderate size exhaust jets. *International Journal of Aeroacoustics*, **9**(4&5), pp. 627-654.
[25] C.-W. Kuo, 2010. Extending acoustic data measured with small scale supersonic model jets to practical aircraft exhaust jets. PhD thesis, the Pennsylvania State University.

Copyright © 2011 by ASME